Greatly enhanced resonant exciton-trion conversion in electrically modulated atomically thin WS_2 at room temperature

By *Zeng Wang*[*], *Matej Sebek, Xinan Liang, Ahmed Elbanna, Arash Nemati, Nan Zhang, Choon Hwa Ken Goh, Mengting Jiang, Jisheng Pan, Zexiang Shen, Xiaodi Su, Nguyen Thi Kim Thanh, Handong Sun, Jinghua Teng*[*]

Dr. Z. Wang, Dr. M. Sebek, Dr. X. Liang, A. Elbanna, Dr. A. Nemati. N. Zhang, Dr. C. H. K. Goh, Dr. M. Jiang, Dr. J. S. Pan, Dr. X. D. Su, Dr. J. H. Teng

Institute of Materials Research and Engineering (IMRE), Agency for Science, Technology and Research (A*STAR), 2 Fusionopolis Way, Innovis #08-03, Singapore 138634, Republic of Singapore

A. Elbanna, Prof. Z. X. Shen, Prof. H. D. Sun

Centre for Disruptive Photonic Technologies, The Photonic Institute, SPMS, Nanyang Technological University, Singapore 637371, Singapore

Division of Physics and Applied Physics, School of Physical and Mathematical Sciences, Nanyang Technological University, Singapore 637371, Singapore

Dr. M. Sebek, Prof. N. T. K. Thanh

Biophysics Group, Department of Physics and Astronomy, University College London, Gower Street, London, WC1E 6BT, UK.

UCL Healthcare Biomagnetics and Nanomaterials Laboratories, 21 Albemarle Street, London, W1S 4BS, UK

*To whom correspondence should be addressed. E-mail: wang_zeng@imre.a-star.edu.sg, or jh-teng@imre.a-star.edu.sg

Abstract

Excitonic resonance in atomically thin semiconductors offers a favorite platform to study 2D nanophotonics in both classical and quantum regimes and promises potentials for highly tunable and ultra-compact optical devices. The understanding of charge density dependent exciton-trion conversion is the key for revealing the underlaying physics of optical tunability. Nevertheless, the insufficient and inefficient light-matter interactions hinder the observation of trionic phenomenon and the development of excitonic devices for dynamic power-efficient electro-optical applications. Here, by engaging an optical cavity with atomically thin transition metal dichalcogenides (TMDCs), we demonstrate greatly enhanced exciton-trion conversion at room temperature (RT) and achieve electrical modulation of reflectivity of nearly 40% at exciton and 7% at trion state, which correspondingly enables a broadband large phase tuning in monolayer tungsten disulfide (WS_2). Besides the absorptive conversion, almost 100% photoluminescence conversion from excitons to trions is observed at RT, illustrating a clear physical mechanism of an efficient exciton-trion conversion for extraordinary optical performance. The results indicate that both excitons and trions can play significant roles in electrical modulation of the optical parameters of TMDCs at RT. The work shows the real possibility for realizing electrical tunable and multi-functional ultra-thin optical devices using 2D materials.

1. Introduction

The development of metasurface in the past decade has affected and transformed many areas of nano-photonics [1-4]. Dynamic light control in metasurfaces [5-10] especially through electrical signal is highly desired and critical for many applications. Multiple mechanisms and materials [11-12] have been reported for tunable and reconfigurable metasurfaces with pros and cons for different applications. For example, chalcogenide-based phase change materials (PCMs) [13] could have large optical constant change responding to electrical pulse [14-16] besides to laser pulse or thermal heating [17-18], but with limitations on the materials loss in the visible range and high-power consumption in reversable tuning mechanism. In fact, the excitonic features in semiconductors are closely linked to their optical behaviors and can be tuned by various methods, such as chemical doping [19], electrical gating [20-22], and thermal effect [23], etc. Different from traditional bulk semiconductors, the enticing properties of excitons in atomically thin transition metal dichalcogenides (TMDCs), such as large exciton binding energy and long lifetime, offer a unique platform for active optical and photonic devices by tuning the exciton resonance at RT [24-30]. Several atomically thin tunable optical devices have been reported solely or partially based on excitonic tuning from TMDCs such as meta-lenses [31], 2D mirrors [32-33], and light modulators [34-37]. However, they either require cryogenic temperature or have insignificant response due to the weak resonance and high optical loss, which hinders the development of TMDCs based compact optical devices operating at RT.

TMDCs have rich kinds of tightly bound quasiparticles [38] such as charged excitons, or trions, which can be converted from excitons via coupling with free charge carriers near the Fermi level. The simultaneous presence of excitons and trions in optoelectronic devices directly affects their properties, making the understanding of trion behavior crucial for optimal device performance [39-41]. Differences in spin splitting, radiative rate, binding energy, and oscillating features between trions and neutral excitons [42-43] reveal that manipulating trionic resonance could be a key aspect in TMDC-based devices when they are electrically doped for optical tuning. However, electrically controlled exciton to trion conversion enabling potentially high performance optical tunable TMDCs devices are rarely studied at RT. The insufficient light-matter interaction strength in the atomic thin TMDCs [44] is a main challenge for observable exciton-trion conversion and evolution at RT. Despite the strong excitonic resonance, the strength of trionic oscillation is much weaker

resulting in a tiny absolute light absorption [31, 36]. The other issue is that the extrinsic loss of current TMDCs based active optical devices is far from ideal for dynamic light control nor enough for detecting trionic signals when not considering a complex van der Waals (vdW) contact or cryogenic temperatures.

Here, we report a greatly enhanced and electrical tunable exciton-trion conversion in monolayer WS_2 at RT by employing a vertical optical cavity with a well-designed Al/Al_2O_3 structure. Via electrostatic gating the monolayer WS_2 with ionic gel, an unprecedented electrical modulation in reflectance of nearly 40% for exciton and 7% for trion states has been experimentally achieved at RT. This accompanies the observation of almost 100% photoluminescence (PL) conversion from excitons to trions without vdW contact. Our electrically gating studies combined with time-resolved PL measurements reveal that the enhanced exciton-trion conversion is the primary source of the large tunability observed at RT. Furthermore, the enhanced conversion also results in large refractive index modulation and large dynamic phase tuning, which will greatly benefit the development of ultra-compact tunable and reconfigurable metasurfaces and metaoptics.

2. Results and Discussion

2.1. Cavity effect to enhance the excitonic resonance of monolayer WS_2

The scheme in Figure 1a shows an optical cavity comprised of an aluminum (Al) layer, a 50 nm thick alumina (Al_2O_3) and a WS_2 monolayer on top. The Al layer is deposited by e-beam evaporation and the Al_2O_3 is deposited via atomic layer deposition (ALD). Like the traditional Si/SiO_2 system, the alumina layer on aluminum conveniently features a strong interfacial adhesion. While, compared to the few percentage excitonic absorption of WS_2 monolayer and the overall

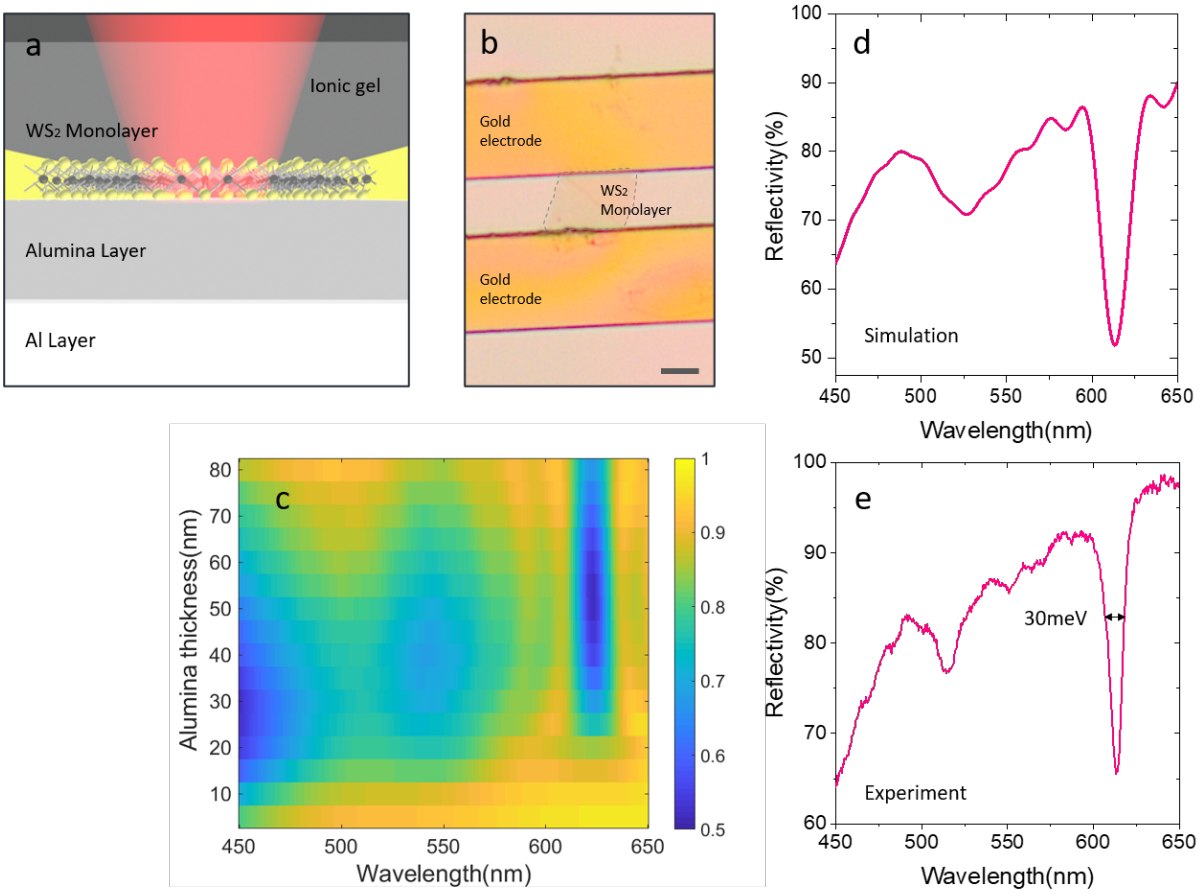

Figure 1. Cavity effect to enhance the excitonic resonance of monolayer WS_2. (a) Schematic of the system with Al/Al_2O_3 and monolayer WS_2. (b) Top-view microscope image of the WS_2 device. (c) Al_2O_3 thickness-dependent excitonic-resonance enhancement of WS_2 monolayer. The color bar represents the value of reflectivity. (d) FDTD simulated reflectivity spectrum of WS_2 device with 50 nm thick Al_2O_3. (e) Experimental reflectivity spectrum of the WS_2 device.

less than 10% device efficiency within Si/SiO_2 system [44], Al/Al_2O_3 system can enable a much stronger excitonic resonance and large absorption at A exciton energy. This cavity effect is also proposed to amplify the trionic resonance during the exciton-trion conversion. The micrograph in Figure 1b shows the flake of the WS_2 monolayer connected to Au electrodes. The monolayer was exfoliated and transferred using the standard viscoelastic stamping [45] and electrodes were fabricated using the photolithography process. The finite difference time domain (FDTD) simulation of the cavity as a function of the alumina thickness in Figure 1c helps to understand the behavior of the optical cavity effect. With a thin alumina layer of 10-30 nm, the spectrum features a strong absorption at the C exciton band around 450 nm, while a thicker alumina layer of 50 nm leads to the enhanced absorption at the A exciton position around 613 nm. The spectrum of the simulated and measured reflectivity of the structure with a 50 nm layer of alumina is shown in Figures 1d and 1e, respectively. The strong excitonic resonance of the A exciton is observed at the wavelength of 613 nm with a depth of 35%. The weaker response is visible in the B exciton range at a wavelength of 514 nm. The measured and simulated spectra are in good agreement except that the A exciton resonance linewidth of 30 meV in the measured spectrum is significantly narrower than the simulated one. The difference is most likely produced by the higher quality of the exfoliated WS_2 monolayer as compared to the tabulated material data used for the simulation.[44] The experimental reflectivity spectrum is normalized to that of the area adjacent to the sample for the absolute optical response of the WS_2 monolayer.

2.2. Deep and multi-level tuning via enhanced exciton-trion conversion

The highly enhanced excitonic resonance opens up space to trigger pronounced exciton-trion conversion and realize deep and multi-level tuning of the resonance at RT. The boosted reflectivity modulation is validated by applying the gate voltage V_g between the reference electrode and the contact electrodes as shown in Figure 2a. It is noted that the two contact electrodes applied from two sides of the WS_2 monolayer flake are connected, which works for a more uniform distribution of the carrier injection during the electrostatic gating. Figure 2b displays that the reflectivity dip at wavelength of 613 nm related to the A exciton resonance is modulated by 40% from $V_g = 0$ to $V_g = 2V$ at RT. This tunability in the visible range tops the performance among the reported experimental results of electro-optical tunable devices based on various 2D materials [31, 35] and even PCMs [14-16]. As the gate voltage is increased, additional free electrons are introduced, leading to the formation of a new excited state of trions. This is evident from the appearance of a fresh

peak at a wavelength of 629 nm and a decrease in the excitonic resonance dip. This finding not only yields a more than 7% modulation in reflectivity at $V_g = 2V$, but it also suggests that trions are excited directly at RT in the doped system, rather than through a dynamic process in which excitons capture a charge and evolve into the trion species. In fact, rare attention has been paid to trions for electro-optical modulation in previous reports since the optical response of trions is rather weak due to the much lower binding energy compared to neutral excitons, especially at RT. Here, thanks to the highly strengthened light-matter interaction, we prove trion can also behave strong absorptive feature at RT and play a key role in optical modulation, which not only extends the active tuning band of TMDCs but also provides an ideal platform to study the many-body effects. The conversion and the resulted large tunability is also experimentally achieved with a monolayer MoS_2 device. The results are shown in Figure S1, which certifies the model of the enhanced exciton-trion conversion with the Al/Al_2O_3 cavity. Figure 2c shows the tunability of the enhanced exciton-trion conversion is highly reproducible and reversible. After switching off the voltage, the device relaxes into the original state and the excitonic resonance evidenced by the deep dip in the reflectivity spectra reemerges. Figure 2d shows the multi-level tuning with different gate voltages, which indicates a controllable exciton-trion conversion. Here we estimate $V_g = 0.5V$ as the charge neutral point from the reflectivity spectra. The position of the minima shows a slight redshift of 1.3 meV at $V_g = 0.5V$, but blueshift at higher voltage reaches 8 meV from 613nm. This is caused by several competing mechanisms. With the excess of free carriers around the charge-neutral regime, the bandgap renormalization effect causes the redshift [34]. Although the Stark effect may have similar effects, we believe it is very weak for monolayer WS_2 due to the tight quantum confinement in the vertical direction. With higher voltage applied, the observed blueshift is mainly caused by two electro-optical effects: 1) the Coulomb screening reduces the exciton binding energy resulting in the blueshifts. 2) the effect of Pauli blocking causes the blueshifts upon the high charge densities ($>10^{13}/cm^2$) brought by the ionic liquid's large capacitance [34], which increases the effective optical bandgap because of an increased number of occupied states within the conduction band upon doping.

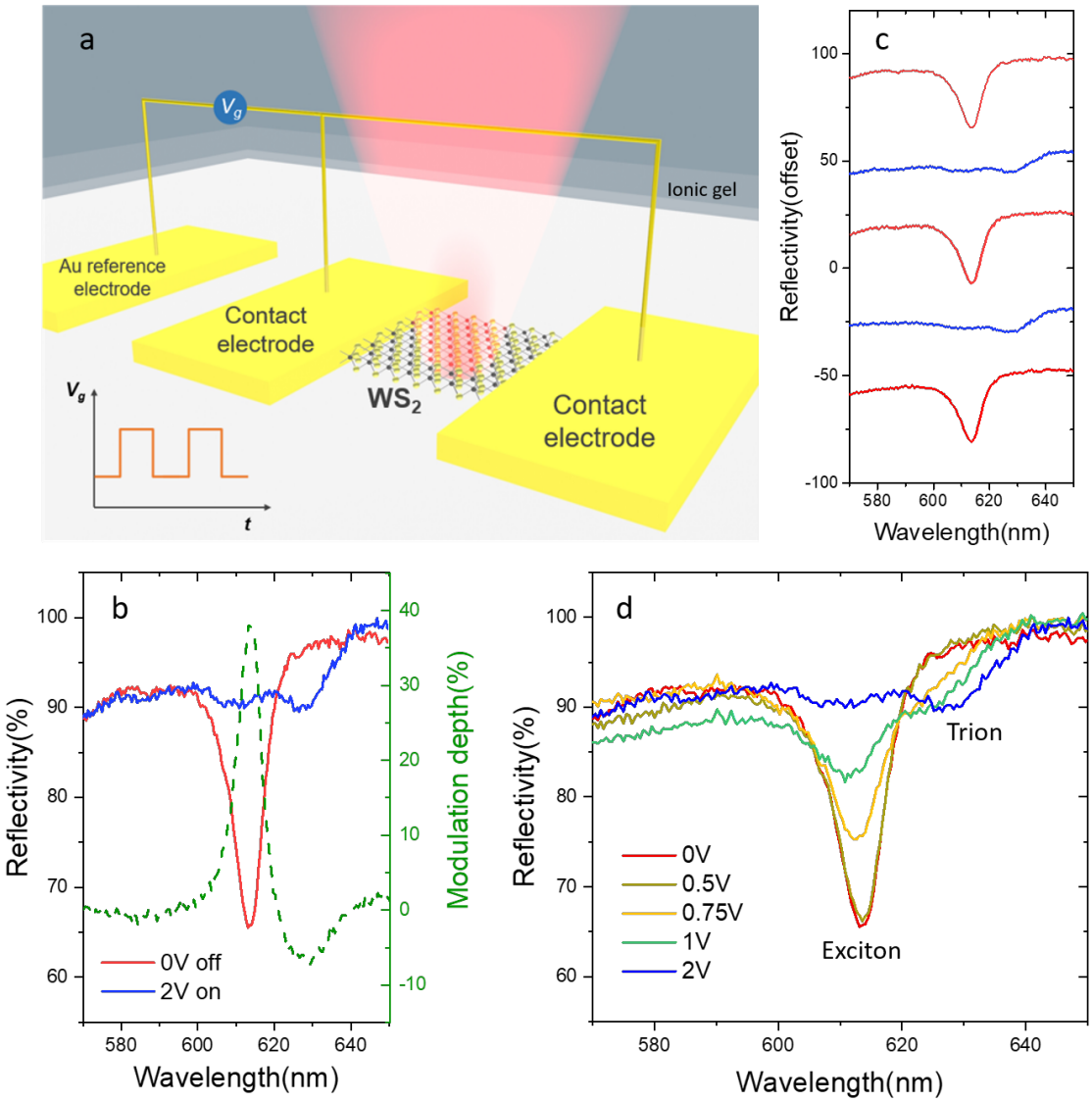

Figure 2. Deep and multi-level tuning of the reflectivity in the WS_2 based device. (a) Schematic of the monolayer WS_2 device with electrode connections. (b) Conversion from enhanced excitonic resonance to trionic resonance, and the corresponding modulation depth. (c) Demonstration of the highly reproducible and reversible tunability of the enhanced excitonic resonance when gate voltage is on (red) and off (blue). (d) Multi-level tuning with different gate voltages enabled by exciton-trion conversion.

2.3. Physical origin of the large tunability

To illustrate and understand the physical mechanism of the excitons-trion conversion that enables the large modulation, we measure the RT PL spectra at different V_g, which is displayed in Figure 3a. At gate voltage near the threshold $V_g = 0.5V$, the injected carrier concentration is very low. As the number of trions is limited by the number of carriers, the concentration of trions is too

low to cause the PL suppression. With higher gate voltage applied, the more carriers injected lead to the decrease of the overall PL intensity and the redshift of PL peak. This phenomenon is analyzed in detail in Figures 3b-e and proved to be a clear exciton-trion conversion.

Without any voltage applied, the PL peak in Figure 3b can be fitted with a single Lorentzian function pointing to a strong neutral exciton emission that is accompanied by the enhanced excitonic resonance dip (dash line). With a voltage above the threshold, the PL spectra in Figures 3c-e can be well fitted with two Lorentzian curves. One peak locates at the wavelength of 615 nm from neutral A exciton emission and the other lower energy peak is attributed to trion emission, which shifts with applied gate voltage. When the gate voltage is much larger than the threshold, the number of injected electrons is large enough and almost all the excitons turn into trions. As a result, the fitting in Figure 3e shows almost a full suppression of PL at A exciton position around 615nm while a strong PL at the wavelength of 632 nm contributed from trions solely. This implies a near-complete exciton-trion conversion at $V_g = 2V$ at RT. Different from neutral excitons, the dominant recombination pathway of trions is non-radiative of which the lifetime was reported as approximately three orders of magnitude shorter than their radiative lifetime. [40] It is worth noting in our study that while the exciton-trion conversion leads to a significant decrease in the overall PL intensity, the absolute PL peaks' counts and integral PL intensity only decrease approximately 100-fold and 50-fold, respectively. This suggests that the radiative recombination rate of trions could be conservatively estimated as only two orders of magnitude lower than their nonradiative recombination rate in our study, considering the negligible nonradiative recombination of exciton in neutral condition. [40] This finding supports a roughly one-order enhancement in trion emission and demonstrates the effectiveness of this cavity in enhancing trionic resonance. The PL mappings at 0 and 2V shown in Figure S4 verify the homogeneity of the sample.

The energy of the trion emission slightly redshifts with higher gate voltage due to the change of Fermi level or the contribution of higher-order many-body effects. [35, 46] The evolution of exciton-trion conversion weakens the excitonic resonance while strengthening the trionic resonance, leading to the modulation of reflectivity of the optical system, as shown in Figures 3b-e. The change of the dips in the reflection spectra is in accordance with the evolution of the peaks in the PL spectra. It is understandable that excitons validate deeper modulation due to their larger binding energy and resonant strength than those of trions, despite the same concentration upon a near-

complete conversion. The exciton-trion conversion process and the electronic band structure are schematically illustrated in Figure 3f. The gate voltage dependent time-resolved PL is shown in Figures 3g and 3h. With the gate voltages of 0 and 0.5V, the decay curves can be fitted well with one exponential function and the lifetimes are 263 ps and 237 ps, respectively, which represents the exciton radiative recombination process and proves the neutral condition of the device. When increasing the gate voltage to 0.75V, the curve includes a fast component around 75 ps and a slow one 484 ps. The decrease in exciton lifetime from 0V to 0.75V is consistent with the expected behavior of excitons in a doping system. Therefore, the fast component is attributed to the exciton radiative recombination process. Then, the slow component could be clearly attributed to the trion radiative recombination, which agrees well with the PL and reflectivity results in Figure 3c. These results indicate another strong proof of the physical origin of the giant tunability. The similar behavior was also reported recently in TMDCs with different doping systems [39, 40, 47, 48], and our results extend the similar feature of trions for 2D optics. Note that because our time-correlated single-photon counting (TCSPC) setup lacks a confocal configuration, the much weaker signal with higher gate voltage is not detectable (more details in optical setup and curve fitting, see supporting information).

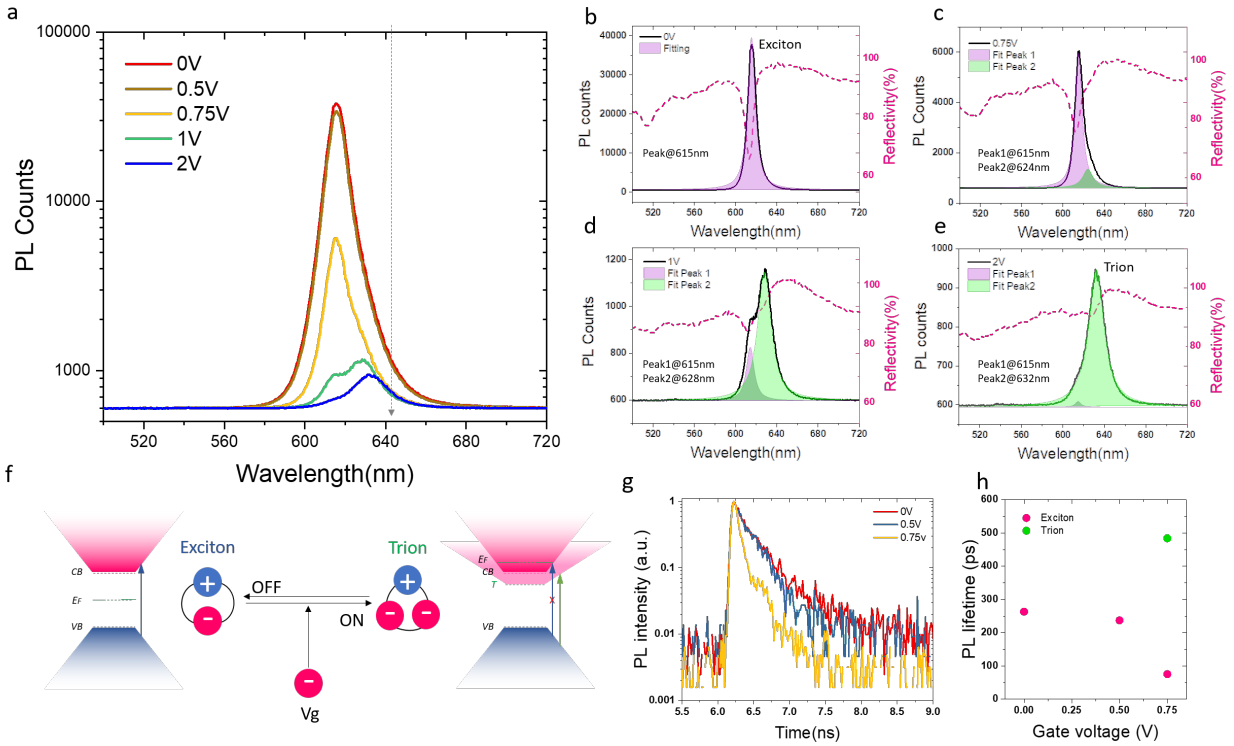

Figure 3. The physical mechanism of exciton-trion conversion that enables the giant modulation. (a) RT PL spectra at different V_g. The Lorentzian fitting of PL spectra and the corresponding reflectivity spectra with (b) $V_g = 0$, (c) $V_g = 0.75V$, (d) $V_g = 1V$, (e) $V_g = 2V$. (f) Schematic of electronic band structures for indicating the photo-physics of the exciton-trion conversion. (g) Time-resolved PL of monolayer WS_2 in the optical device at different V_g of 0V, 0.5V and 0.75V. (h) Lifetime fitting based on the time-resolved PL at different V_g.

2.4. Large refractive index modulation

A key factor in the tunable and reconfigurable meta-optics is the ability of phase tuning. We employ the tunable reflectivity spectra to analyze the complex refractive index modulation of the WS_2 monolayer, which helps to explore the possibility of dynamic phase tuning in the same structure. Kramers-Kronig analysis is used in combination with the transfer matrix method to obtain the complex refractive index. Using the least square method, we minimized the difference between the measured reflectivity spectra and those calculated with the transfer matrix method while fitting the dielectric function of the WS_2 monolayer. The imaginary part of the dielectric function ε_i is fitted with multiple Lorentzians in the form:

$$\varepsilon_i(E) = \sum_j \frac{f_j E \gamma_j}{\left(E_j^2 - E^2\right)^2 + E^2 {\gamma_j}^2} \qquad (1)$$

Where f_j is the oscillator strength, E_j is the central energy and γ_j is the full width at half maximum of the j-th oscillator. The real part ε_r is then calculated with the Kramers-Kronig relation:

$$\varepsilon_r(E) = -\frac{1}{\pi}\int_{\omega_2}^{\omega_1} \frac{\varepsilon_i(E')}{E' - E} dE' + C \qquad (2)$$

where ω_1 and ω_2 denote limits of our measurement and the integration constant C is estimated from the dielectric function of the bulk WS_2 [49, 50]. The fitting curves match perfectly with our experimental data (for details see Supporting Information Figure S8). The complex refractive index is then calculated from the fitted dielectric function as follows: $n + i\kappa = \sqrt{\varepsilon_r + i\varepsilon_i}$. The derived carrier density dependent tunable complex refractive index is showed in Figures 4a and 4b. The results translate to a substantial 75% tunability in the imaginary part and 25% in the real part of the refractive index at RT, indicating the modulation works for both amplitude and phase. The accumulated carrier density is calculated by the equation $\Delta n_{WS2} = C \times (V_g - V_{neutral})/e$, where C is the capacitance of the ion gels and takes the value of 5.7 μF cm^{-2} from previous reports [34]. $V_{neutral} \approx 0.5$V is determined by reflectivity and PL spectra.

For a better understanding of the underlying physics, we derived the oscillator strength f, bandwidth γ, and the resonant energy E for both excitons and trions on the variation of gate voltage, which is shown in Figure 4e, 4f and 4g. It can be noted in equations (1) and (2) that with no obvious changes in resonant energy or wavelength at different voltages, the f/γ determines the tunability of the whole system. Different from the previously reported system [36], the cavity effect of Al/Al_2O_3

enables the initial f as high as 1.75 and the γ as narrow as 30 meV, which generates a giant tunable space when the exciton to trion conversion happens. For comparison, we prepared a sample replacing the Al with Si substrate and keeping other parameters the same, as shown in Figure S9. This formation results a broadening of exciton bandwidth to around 50 meV, which is similar to a previous report [36]. With the voltage applied to our device structure, the f drops to 1, and the γ broadens to nearly 80 meV for the exciton, resulting in the giant tunability at the on-resonance state. More interestingly, due to the cavity effect, the generated trions show an even narrower bandwidth accompanied by a relatively strong oscillator strength, which is rarely observed at RT while consistent with its largely enhanced dips in the reflectivity spectra in Figure 2b. In fact, measuring reflectivity accurately and reliably for trions in ultrathin samples under electrostatic doping is challenging due to weak light-matter interactions. Direct absorption measurements to estimate the WS_2 trion binding energy have only been reported below 50 K using hBN encapsulated samples [51]. However, the resonant peaks of reflectance shown in Figure 4g allow for a clear determination of trion binding energy at room temperature due to the cavity effect. Under slightly N-doped conditions with $V_g = 0.75$V, the trion binding energy can be calculated to be around 42 meV, as evidenced by limited trion PL signal compared with exciton PL counts. At $V_g = 2$V, larger Fermi energies result in a value as large as 59 meV. By linearly fitting the trion energies under different voltages, the trion binding energy of zero voltage limit can also be estimated to be around 35 meV. This demonstration of trion binding energy is expected to advance the understanding of trion physics at room temperature and indicate the optical cavity used in our work can highly enhance the on-resonance states of both excitons and trions, making the exciton-trion conversion more pronounced for applications.

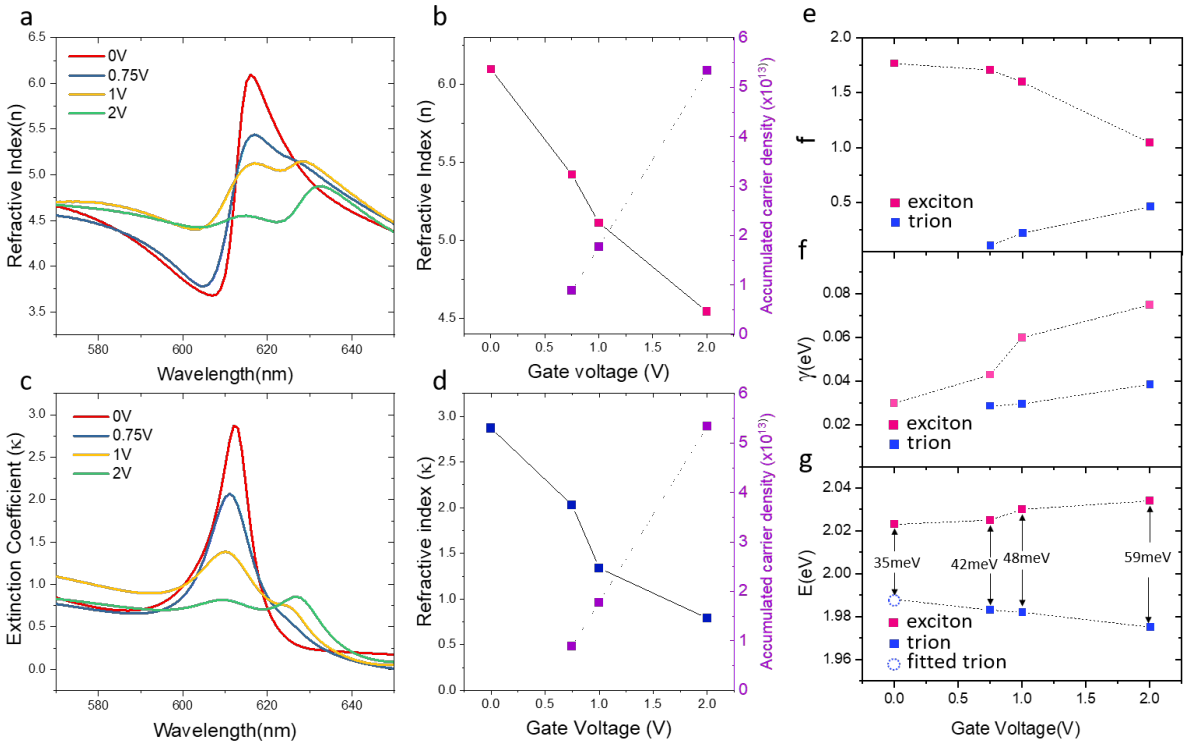

Figure 4. Large refractive index modulation. (a) The refractive index n of the monolayer WS_2 and, (b) The relation between the tuning of the *n* and the accumulated carrier density with different voltages. (c) The extinction coefficient κ of the monolayer WS_2 and, (b) The relation between the tuning of the κ and the accumulated carrier density with different voltages. Tuning in (e) oscillator strength *f*, (f) bandwidth γ, (g) resonance energy *E* for excitons, trions and its binding energies, as a function of gate voltage.

2.5. Electrical phase tuning by the monolayer WS_2 device

Phase modulation with a small optical volume is essential for advancing dynamic meta-optics and metasurfaces. An electrical tuning solution with an efficient and deep modulation is still a grand challenge, especially in the visible range at RT.

Thanks to the highly enhanced exciton-trion conversion in monolayer WS_2 with the efficient Al/Al_2O_3 cavity effect, here we demonstrate a feasible pathway for broadband dynamic phase modulation. A home-built Michaelson interferometer optical setup together with a five-step temporal phase stepping algorithm [52, 53] is used to obtain the phase information of the sample before and after the voltage applied, which is shown in Figure 5a (details of this setup and data processing see the Supplementary Information). As displayed in Figure 5b, we have experimentally achieved a dynamic phase tuning in wavelength range of 600 nm to 650 nm with

the largest phase shift up to 0.2π in a sub-nanometer film under 2V voltage, which locates at 605 nm near the excitons' resonant peak and originates from the tuning of the real part of the device's dielectric function. Moreover, the tunable range could be extended to 650 nm thanks to the trions' resonance. In order to indicate the conversion behavior between the excitons and trions in the phase domain, we plot the reflectivity and phase tuning together for comparison. It can be seen that both the excitons and trions contribute to the phase tuning. Importantly, due to the conjugate feature between the n and k, the experimental results show clear conjugate tuning between the amplitude and phase for both exciton and trion resonant peaks, which is shown in Figure 5c. Besides, the all-above 90% reflectivity of the tuning wavelengths indicates an ideal device efficiency. These results could be greatly favored by the active metasurface designers because either amplitude or phase is stable when the other is used for tuning.

a

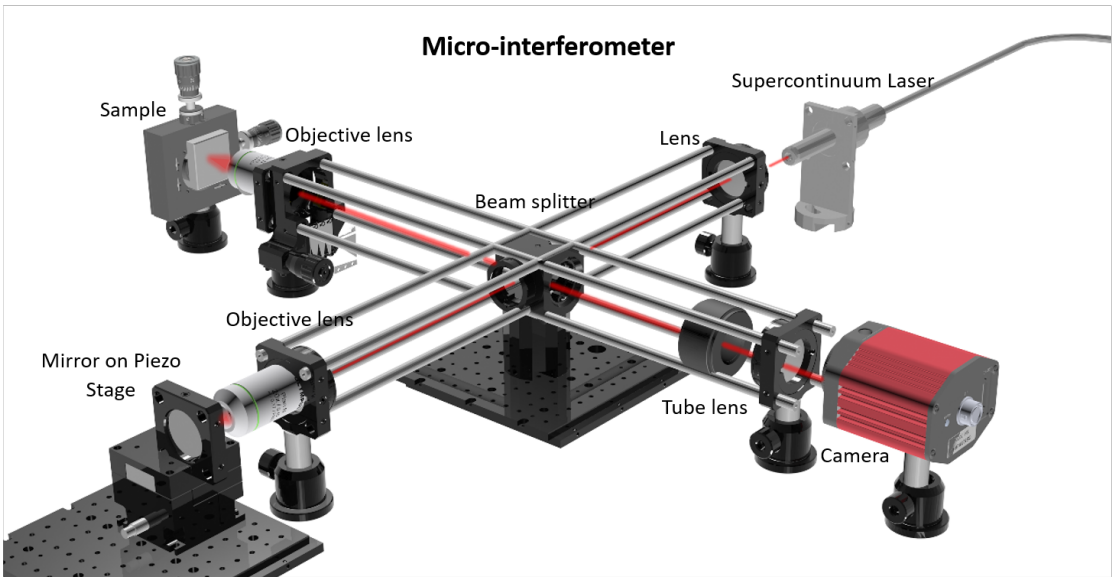

b

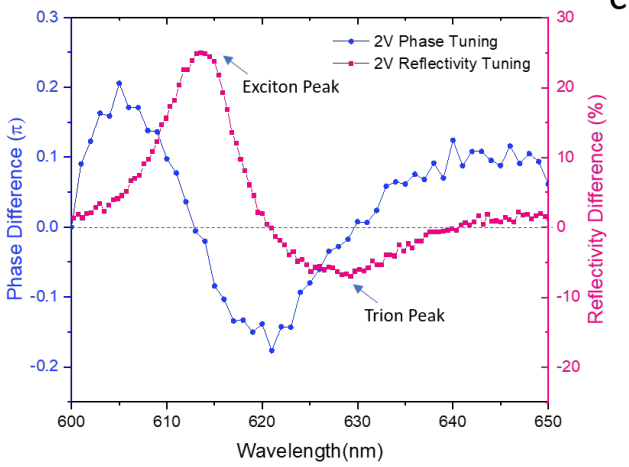

c

Wavelength	Reflectivity Tuning	Phase Tuning	On-State Reflectivity
605nm	4.5%	0.2π	90.6%
613nm	26%	0	90.4%
621nm	0	0.17π	91.1%
629nm	7%	0	90.0%
639nm	0	0.1π	98.1%

Figure 5. Dynamic phase tuning with enhanced excitonic and trionic resonances in monolayer WS_2. (a) The schematic of the home-built micro-interferometer that measures the dynamic phase tuning. (b) Experimental phase difference of the monolayer WS_2 device measured by our home-built micro-interferometer and the correlated reflectivity difference. (c) Conjugate tuning between the amplitude and phase for both exciton and trion resonant peaks.

3. Conclusion

In conclusion, we have demonstrated highly enhanced resonant conversion between exciton and trion in TMDCs at RT with Al/Al2O3 cavity effect. With monolayer WS_2, we experimentally achieved a 40% amplitude modulation in exciton resonance and 7% in trion. A giant and broadband phase tuning up to 0.2π in sub-nanometer 2D film with a high reflectivity is demonstrated. A near-complete resonant conversion from fully contributed by excitons to fully by trions is proved by the PL evolution at RT and is responsible for the large electrical tunability in reflectivity and the refractive index. Our findings not only reveal a clear resonant conversion between excitons and trions but also demonstrate that trions play a key role in the electrical tuning of TMDCs devices even at RT. These results enrich the understanding of the electro-optical properties of 2D TMDCs and greatly benefit the development of next generation tunable ultra-compact nano-optics and photonics.

4. Experimental Section

Materials and sample preparation*:* WS_2 crystals were purchased from HQ graphene. Sapphire was used as a substrate. 100 nm of aluminum was deposited using Denton Explorer e-beam evaporator at a deposition rate of 0.5 Å/s followed by a deposition of 50 nm alumina using Beneq TFS 200 ALD system with H_2O and TMA as precursors. The alumina was grown at 120 degrees with 15 seconds purge time and 200 ms of pulse time for the duration of 455 cycles. The thickness of the alumina layer was determined with ellipsometry as 49.7 nm. All 2D TMDCs samples were prepared using exfoliation on PDMS and viscoelastic stamping described elsewhere. [34] Standard photolithography with AZ5214 photoresist spin-coated for 30 s at 6000 rpm was used for the contact patterning in a SUSS Mask Aligner MA6 with contact pitch corresponding to the flake size.

Optical characterization*:* PL spectra were measured using WITec Alpha 300R confocal microscope. A 532-nm CW pump laser focused by a ×100 microscope objective lens (NA=0.9) was used for excitation and the PL signal was collected with the same objective. A diffraction grating with 150 lines/mm was used. A thermoelectrically cooled coupled charged device was used

for the detection. Spectra were averaged from 10 measurements with the integration time of 0.1s. Reflectivity measurements were performed using CRAIC 20/30PV. For each measurement, 15 measured spectra were averaged. The electrical bias was applied using Keithley 2450 source meter. The modulation depth is defined as the relative change in the reflectivity intensity, which can be expressed as $\Delta R/R_0$. Here, R_0 represents the reflectivity of off-state.

Ionic gel preparation: The ionic gel was prepared using a method described elsewhere[1]. Briefly, the triblock co-polymer poly (styrene block-methyl methacrylate block-styrene) (PS-PMMA-PS) and the ionic liquid 1-ethyl3-methylimidazolium bis (trifluoromethylsulfonyl) imide (EMIM-TFSI) were added into ethyl propionate at a weight ratio of 0.7:9.3:90. To dissolve the polymer, we heated the solution to 50 degrees. The gel was then spin-coated on the sample for 30 seconds at 6000 rpm and let the solvent evaporate at RT. Chips were wire-bonded after the ion gel spin-coating. It is worth noting that the gel can be easily removed by dissolving in ethyl propionate.

Finite difference time domain simulation*:* In evaluating the optimized Al/Al_2O_3 system with TMDCs films, we utilized the FDTD method to carry out the numerical simulations. The 12 perfect matching layers (PMLs) were employed along the directions to avoid the undesired reflection from the boundaries. The periodic conditions were used in x and y directions. Because the thickness (from hundreds of micrometers to several millimeters) of the real substrate is too large for the FDTD model, we just simulated the contacting part between the film and substrate by setting the light source in the substrate. Thus, our simulated transmission of the sample had ignored the reflection from the bottom surface of the substrate. So, our simulated reflection was defined as the ratio of the reflected power recorded by the detector to the total power of the incident light source. In our model, the detector was set 0.5 μm away from the top surface of the substrate, so that no evanescent wave was involved in the calculated transmission. Due to the ultra-small thickness of the 2D films, we used a fine grid of 0.25 nm along z direction within the films, so as to reduce the simulation error. In our simulation, all the WS_2 materials had the experimental refractive indices imported in the sampling data base for simulation.

Supporting Information: supporting information is available from the Wiley Online Library or from the author.

Acknowledgements: Z.W. and M.S. contribute equally to this work. The project is financially supported by A*STAR under IRG program (Grant numbers A20E5c0084 and A2083c0058) and the National Research Foundation, Singapore under NRF-CRP (NRF-CRP26-2021-0004)

Competing financial interests: The authors declare no competing financial interests.

Data Availability Statement: The data that support the findings of this study are available from the corresponding author upon reasonable request

Keywords: exciton, trion, exciton-trion conversion, electro-optical modulation, transition metal dichalcogenides, 2D materials, tunable metasurface, tunable metaoptics, electrically tunable metaoptics

References

[1] D. Smith, J. Pendry, M. Wiltshire, *Science* **2004**, *305*, 788.

[2] I. Staude, J. Schilling, *Nature Photonics* **2017**, *11*, 274.

[3] S. Jahani, Z. Jacob, *Nature Nanotechnology* **2016**, *11*, 23.

[4] N. Yu, F. Capasso, *Nature Materials* **2014**, *13*, 139.

[5] A. M. Shaltout, V. M. Shalaev, M. L. Brongersma, *Science* **2019**, 364.

[6] J. Park, B. G. Jeong, S. I. Kim, D. Lee, J. Kim, C. Shin, C. B. Lee, T. Otsuka, J. Kyoung, S. Kim, K.-Y. Yang, Y.-Y. Park, J. Lee, I. Hwang, J. Jang, S. H. Song, M. L. Brongersma, K. Ha, S.-W. Hwang, H. Choo, B. L. Choi, *Nature Nanotechnology* **2020**, 16, 69.

[7] V. E. Babicheva, A. Boltasseva, A. V. Lavrinenko, *Nanophotonics* **2015**, 4, 165.

[8] Z. Wang, Y. Wang, G. Adamo, B. Teh, Q. Wu, J. Teng, H. Sun, *Advanced Optical Materials* **2016**, *4*, 883.

[9] C. Enkrich, M. Wegener, S. Linden, S. Burger, L. Zschiedrich, F. Schmidt, J. Zhou, T. Koschny, C. Soukoulis, *Physical Review Letters* **2005**, *95*, 203901.

[10] Q. Zhao, J. Zhou, F. Zhang, D. Lippens, *Materials Today* **2009**, *12*, 60.

[11] A. Nemati, Q. Wang, M. Hong, J. Teng, *Opto-Electronic Advances* **2018**, 1, 18000901.

[12] Elena Mikheeva, Christina Kyrou, Fouad Bentata, Samira Khadir, Sébastien Cueff, and Patrice Genevet, "Space and Time Modulations of Light with Metasurfaces: Recent Progress and Future Prospects," *ACS Photonics*, **2022**, *9*, 1458.

[13] C. Zheng, R. E. Simpson, K. Tang, Y. Ke, A. Nemati, Q. Zhang, G. Hu, C. Lee, J. Teng, J. K. W. Yang, J. Wu, C.-W. Qiu, *Chemical Reviews* **2022**, 122, 15450.

[14] S. Lepeshov, A. Krasnok, *Nature Nanotechnology* **2021**, *16*, 615.

[15] Y. Zhang, C. Fowler, J. Liang, B. Azhar, M. Shalaginov, S. Deckoff-Jones, S. An, J. Chou, C. Roberts, V. Liberman, M. Kang, C. Ríos, K. Richardson, C. Rivero-Baleine, T. Gu, H. Zhang, J. Hu, *Nature Nanotechnology* **2021**, *16*, 661.

[16] Y. Wang, P. Landreman, D. Schoen, K. Okabe, A. Marshall, U. Celano, H. Wong, J. Park, M. Brongersma, *Nature Nanotechnology* **2021**, *16*, 667.

[17] A. Nemati, G. Yuan, J. Deng, A. Huang, W. Wang, Y. T. Toh, J. Teng, Q. Wang, *Advanced Optical Materials* **2022**, 10, 2101847.

[18] Q. Wang, E. T. Rogers, B. Gholipour, C.-M. Wang, G. Yuan, J. Teng, N. I. Zheludev, *Nature Photonics* **2015**, 10, 60.

[19] X. Zhang, L. Li, Z. Sun, J. Luo, *Chemical Society Reviews* **2019**, *48*, 517.

[20] A. Liu, R. Jones, L. Liao, D. Samara-Rubio, D. Rubin, O. Cohen, R. Nicolaescu, M. Paniccia, *Nature* **2004**, *427*, 615.

[21] J. Han, F. Boeuf, J. Fujikata, S. Takahashi, S. Takagi, M. Takenaka, *Nature Photonics* **2017,** *11*, 486.

[22] D. Janner, D. Tulli, M. García-Granda, M. Belmonte, V. Pruneri, *Laser & Photonics Reviews* **2009**, 3, 301.

[23] Y. Liu, Y. Yang, D. Shi, M. Xiao, L. Jiang, J. Tian, G. Zhang, Z. Liu, X. Zhang, D. Zhang, *Advanced Materials* **2019**, *31*, 1902576.

[24] K. Mak, J. Shan, *Nature Photonics* **2016**, *10*, 216.

[25] Z. Wang, G. Yuan, M. Yang, J. Chai, Q. Steve Wu, T. Wang, M. Sebek, D. Wang, L. Wang, S. Wang, D. Chi, G. Adamo, C. Soci, H. Sun, K. Huang, J. Teng, *Nano Letters* **2020**, *20*, 7964.

[26] M. Brongersma, *Nanophotonics* **2020**, *10*, 643.

[27] Y. Wang, Z. Deng, D. Hu, J. Yuan, Q. Ou, F. Qin, Y. Zhang, X. Ouyang, Y. Li, B. Peng, Y. Cao, B. Guan, Y. Zhang, J. He, C. Qiu, Q. Bao, X. Li, *Nano Letters* **2020**, *20*, 7811.

[28] A. Dasgupta, J. Gao, X. Yang, *Nano Letters* **2019**, *19*, 6511.

[29] J. Yang, Z. Wang, F. Wang, R. Xu, J. Tao, S. Zhang, Q. Qin, B. Luther-Davies, C. Jagadish, Z. Yu, Y. Lu, *Light: Science & Applications* **2016**, *5*, e16046.

[30] F. Qin, B. Liu, L. Zhu, J. Lei, W. Fang, D. Hu, Y. Zhu, W. Ma, B. Wang, T. Shi, Y. Cao, B. Guan, C. Qiu, Y. Lu, X. Li, *Nature Communications* **2021**, *12*, 1.

[31] J. van de Groep, J. Song, U. Celano, Q. Li, P. Kik, M. Brongersma, *Nature Photonics* **2020**, *1,* 426.

[32] P. Back, S. Zeytinoglu, A. Ijaz, M. Kroner, A. Imamoğlu, *Physical review letters* **2018**, *120,* 037401.

[33] Y. Zhou, G. Scuri, J. Sung, R. Gelly, D. Wild, K. De Greve, A. Joe, T. Taniguchi, K. Watanabe, P. Kim, M. Lukin, H. Park, *Physical Review Letters* **2020**, *124*, 027401.

[34] J. Pu, K. Matsuki, L. Chu, Y. Kobayashi, S. Sasaki, Y. Miyata, G. Eda, T. Takenobu, *ACS Nano* **2019**, *13*, 9218.

[35] M. Li, S. Biswas, C. Hail, H. Atwater, *Nano Letters* **2021**, *21*, 7602.

[36] Y. Yu, Y. Yu, L. Huang, H. Peng, L. Xiong, L. Cao, *Nano Letters* **2017**, *17*, 3613

[37] I. Datta, S. Chae, G. Bhatt, M. Tadayon, B. Li, Y. Yu, C. Park, J. Park, L. Cao, D. Basov, J. Hone, M. Lipson, *Nature Photonics* **2020**, *14*, 256.

[38] K. Mak, K. He, C. Lee, G. Lee, J. Hone, T. Heinz, J. Shan, *Nature Materials* 2012, *12*, 207.

[39] P. Chen, T. Atallah, Z. Lin, P. Wang, S. Lee, J. Xu, Z. Huang, X. Duan, Y. Ping, Y. Huang, J. Caram, X. Duan, *Nature* **2021**, *599*, 404.

[40] D. Lien, S. Uddin, M. Yeh, M. Amani, H. Kim, J. Ager, E. Yablonovitch, A. Javey, *Science* **2019**, *364*, 468.

[41] M. G. Harats, J. N. Kirchhof, M. Qiao, K. Greben, K. I. Bolotin, *Nature Photonics* **2020**, 14, 324.

[42] J. S. Ross, S. Wu, H. Yu, N. J. Ghimire, A. M. Jones, G. Aivazian, J. Yan, D. G. Mandrus, D. Xiao, W. Yao, X. Xu, *Nature Communications* **2013**, 4.

[43] Q. Zhang, H. Sun, J. Tang, X. Dai, Z. Wang, C.-Z. Ning, *Nature Communications* **2022**, 13.

[44] Y. Li, A. Chernikov, X. Zhang, A. Rigosi, H. M. Hill, A. M. Van Der Zande, D. A. Chenet, E. Shih, J. Hone, T. F. Heinz, *Physical Review B* **2014**, *90*, 205422.

[45] A. Castellanos-Gomez, M. Buscema, R. Molenaar, V. Singh, L. Janssen, H. van der Zant, G. Steele, *2D Materials* **2014**, *1*, 011002.[46] J. Shang, X. Shen, C. Cong, N. Peimyoo, B. Cao, M. Eginligil, T. Yu, *ACS Nano* **2015**, *9*, 647.

[47] J. Shi, Y. Li, Z. Zhang, W. Feng, Q. Wang, S. Ren, J. Zhang, W. Du, X. Wu, X. Sui, Y. Mi, R. Wang, Y. Sun, L. Zhang, X. Qiu, J. Lu, C. Shen, Y. Zhang, Q. Zhang, X. Liu, *ACS Photonics* **2019**, 6, 3082.

[48] J. Shi, J. Zhu, X. Wu, B. Zheng, J. Chen, X. Sui, S. Zhang, J. Shi, W. Du, Y. Zhong, Q. Wang, Q. Zhang, A. Pan, X. Liu, *Advanced Optical Materials* **2020**, 8, 2001147.

[49] A. R. Beal, W. Y. Liang, H. P. Hughes, *Journal of Physics C: Solid State Physics* **1976**, *9*, 2449.

[50] E. D. Palik, ed. *Handbook of optical constants of solids.* Vol. 3. Academic press, **1998.**

[51] A. Arora, T. Deilmann, T. Reichenauer, J. Kern, S. Michaelis de Vasconcellos, M. Rohlfing, R. Bratschitsch, *Physical review letters* **2019**, 123, 167401.

[52]. C. Joenathan, *Applied optics* **1994**, *33*, 4147.

[53]. X. Liang, Y. Yu, X. Xu, Y. Fu, V. Valuckas, R. Paniagua-Dominguez, A. Kuznetsov, Applied Optics **2021**, *61*, B164.